Journal of Materials Chemistry

Cite this: J. Mater. Chem., 2012, 22, 6267

www.rsc.org/materials

PAPER

Morphological control of platinum nanostructures for highly efficient dye-sensitized solar cells†

Lu-Lin Li,* Chia-Wei Chang, Hsin-Hui Wu, Jia-Wei Shiu, Po-Ting Wu and Eric Wei-Guang Diau*

Received 24th November 2011, Accepted 17th January 2012
DOI: 10.1039/c2jm16135d

Cyclic electro-deposition (CED) is a cost-effective tool to synthesize nanostructures with a solution process, controllable morphology and high purity. Here we report novel platinum nanostructures fabricated according to CED at room temperature in solution containing H_2PtCl_6 precursor and $NaNO_3$. Remarkable Pt nanostructures—from nanoclusters, nanosheets, nanograsses to nanoflowers—were produced through morphological control *via* variation of either period of CED scans or concentration of the precursor. Pt films with uniform nanograss structures have great electro-catalytic performance (electron-transfer resistance = 0.3 Ω) and intrinsic light-scattering (reflectivity ~50%), perfectly suitable for use as counter-electrodes for dye-sensitized solar cells (DSSCs). The DSSC device made with the Pt-nanograss counter-electrode and N719 dye attained efficiency η = 9.61% of power conversion, which is 12% enhanced from that fabricated according to a conventional thermal decomposition method (η = 8.55%) under similar experimental conditions. When the devices were further optimized with a thick TiO_2 film (17 + 5 μm) sensitized by Z907 dye using the CED-Pt counter-electrode, we obtained J_{SC} (mA cm^{-2}) = 19.44, V_{OC} (V) = 0.742, and FF = 0.736, giving an exceptional power conversion efficiency of 10.62%.

1. Introduction

Regarded as a promising candidate for the next-generation photovoltaic devices, the dye-sensitized solar cell (DSSC) has attracted much attention in a search for cheap key materials to promote its performance.[1–4] In a DSSC, electrons radiatively excited from a sensitizer are rapidly injected into the conduction band of TiO_2, and then transferred to catalytically activated counter electrodes (CEs) through exterior electric circuits. Holes are released from the dye cations to the I^-/I_3^- redox couple in the electrolyte, and then transported to the CE. To improve the cell performance, much effort has been focused on the design and synthesis of novel sensitizers with large absorption coefficients[5–7] and on photoanode materials with large surface area and efficient electron diffusion.[8,9] The CE is an important component in optimization of the cell performance, especially to sustain devices with highly loaded sensitizers or limitation due to mass transfer of the electrolyte.[9,10] In general, the reduction, $I_3^- + 2e^- \rightarrow 3I^-$, occurs at the CE/electrolyte interface to provide sufficient iodide anions for dye regeneration. To improve the catalytic activity at the surface of the transparent conducting oxide (TCO) substrate of the CE, the TCO surface is modified with a thin layer of electro-catalyst to increase the rate of reduction.[10–12]

For this purpose, promising materials, such as platinum (Pt),[13,14] carbon nanostructures,[15–18] conducting polymers,[19] surface-nitrided nickel,[20] and TiN,[21,22] were fabricated on TCO glass or metallic foil substrates because of their superior electro-catalytic activity and satisfactory electrical conductivity. Efficient CE materials NiS,[23] molybdenum carbide and tungsten carbide[24] are reported; all materials exhibit catalytic activities comparable with that of Pt. Among them platinum is the electro-catalyst favoured for a counter electrode because of its excellent catalytic performance and chemical and thermal stability. To improve the cell performance, platinized counter electrodes have been obtained by diverse synthetic approaches, including sputtering deposition (SD),[13,25–27] thermal decomposition (TD) at high temperature,[10,11] electrochemical deposition,[28–30] electrodeless deposition[31] and chemical reduction.[32–34] For instance, using a chemical-reduction method, Sun *et al.*[32] prepared an efficient DSSC device with a polyol reduced Pt CE (η = 8.1%); Chen *et al.*[33] fabricated a Pt film reduced with $NaBH_4$ under hydro-thermal conditions at 100 °C as CE materials for flexible DSSC applications (η = 5.4%).

Great electro-catalytic activity and satisfactory conductivity are two major characteristics to be considered for CE materials to decrease efficiently the charge-transfer resistance (R_{CT}) and the overpotential at the interface of Pt and electrolyte.[32] Another

Department of Applied Chemistry and Institute of Molecular Science, National Chiao Tung University, No. 1001, Ta Hsueh Rd, Hsinchu 30010, Taiwan. E-mail: llli@mail.nctu.edu.tw; diau@mail.nctu.edu.tw; Fax: +886-3-572-3764; Tel: +886-3-5131524

† Electronic supplementary information (ESI) available: CV scans for the electro-deposition of Pt, SEM images of TD-Pt, SD-Pt and Pt films electrodeposited without $NaNO_3$, photovoltaic performances of CED-nanocluster-Pt, optimized conditions to prepare TD-Pt and SD-Pt films. See DOI: 10.1039/c2jm16135d

promising approach is a rational design of the CE surface by introducing a reflecting layer, such as a photonic crystal[35] or a metallic mirror,[36,37] to reflect the unabsorbed photons back into the photoanode to improve the light-harvesting efficiency of the solar cells. With a sputtering technique, Grätzel and co-workers employed a Pt mirror of thickness 2 μm as a light-reflecting CE.[36,37] Although the light-harvesting efficiency is improved on reflecting light back from a Pt mirror, it is an expensive approach because it requires much Pt-loading on the TCO surface. Moreover, according to the work of Fang *et al.*,[25] the electro-catalytic performance of a sputtered Pt CE is not improved with a Pt film of thickness greater than 10 nm. Similar results have also been reported by Ho and co-workers.[38] According to Ho's results, the R_{CT} decreases with increasing the deposition time until 30 s; the R_{CT} values and the catalytic performance remain the same for further sputtering deposition, showing an independent behavior of Pt-loading on device performance.

To attain both sufficient electro-catalytic and light-reflective features in one material with a small Pt-loading, we propose a design for the fabrication of a high-performance Pt CE with shape controlled with various nanostructural morphologies based on cyclic electro-deposition (CED) in an electrolyte solution containing precursor H_2PtCl_6 and $NaNO_3$. The morphologies of the Pt layers are controllable to show nanocluster, nanosheet, nanograss and nanoflower features in a systematic way, depending on the periods of the CED scans or the concentrations of the precursor H_2PtCl_6 in the presence of $NaNO_3$. A DSSC device prepared according to this CED approach for a CE made of uniform nanograss structure (Pt-nanograss) exhibits notable photovoltaic performance (η = 9.61%) superior to the devices for those CEs prepared with an expensive SD method (η = 8.77%) or with a conventional TD method (η = 8.55%) under similar fabrication conditions.

2. Experimental

2.1 Fabrication of Pt counter electrodes

(1) CED method. Electro-deposition was performed with an electrochemical system (IM 6, Zahner) and three electrodes near 295 K, a Pt coil as the counter electrode, Ag/AgCl as the reference electrode and an indium-doped tin-oxide (ITO, 2.8 Ω $\square^{-1}$) glass substrate as the working electrode (total area 1 × 2 cm^2, active area 1 × 1 cm^2). For synthesis of Pt counter electrodes with nanocluster, nanograss and nanoflower structures, the ITO substrates were immersed into a stock solution ($NaNO_3$ 5 mM, H_2PtCl_6 1.0, 1.5, 2.5, 5.0, 7.5, 12.5 mM) in ultrapure water (18 MΩ) using cyclic electro-deposition with potential controlled in a range −1.0 to 0.2 V at scan rate 0.05 V s^{-1} for 2–15 cycles. The films as prepared were rinsed with ethanol to remove all residue and dried with gaseous N_2.

(2) SD method. The sputtering-deposited platinized counter electrode was fabricated on depositing platinum onto ITO glass substrates with a d.c. magnetron sputtering instrument. Upon optimizing the sputtering condition, we employed an input power density of 2 W cm^{-2} in gaseous Ar at 0.5 Pa for 5.5 min.

(3) TD method. Thermally decomposed platinized counter electrode was prepared with a conventional thermal reduction.[10,11] A platinum-containing solution (H_2PtCl_6 in isopropanol) was spin-coated onto ITO glass at 2000 rpm for 10 s. The film as deposited was heated at 380 °C for 30 min. By repeating the thermal decomposition process for 2 times to reach the optimal condition (Fig. S1, ESI†), the Pt-CEs were fabricated for comparison. The surface morphologies of these Pt films were observed with a field-emission scanning electron microscope (SEM, JEOL JSM-6390LV). Reflection spectra of the CE were recorded on a UV/vis/NIR spectrometer (V-570, Jasco).

2.2 Electrochemical measurements

Electrocatalytic measurements of the tri-iodide reduction were performed in CH_3CN solution (LiI 0.01 M, I_2 0.001 M, $LiClO_4$ 0.1 M) at scan rate 100 mV s^{-1} using cyclic voltammetric (CV) analysis. Electrochemical impedance spectra (EIS) were measured with an electrochemical system (IM 6, Zahner) in a symmetrical cell design. Two identical platinized electrodes were assembled and sealed with a hot-melt film (SX1170, Solaronix, thickness 25 μm, active area 0.45 × 0.45 cm^2). The measured frequency range was 10 mHz to 0.2 MHz; the magnitude of alternating potential was 10 mV. The EIS data were analyzed with an appropriate equivalent circuit using Z-view simulation software.

2.3 Device fabrication

TiO_2 nanoparticles were prepared with a sol–gel method reported elsewhere.[39] A paste composed of TiO_2 NP (particle size ~20 nm) was coated with screen printing on a $TiCl_4$-pretreated FTO glass (TEC7, Hartford, USA). A scattering layer (particle size 200–600 nm) was screen-printed additionally on the active layer to improve the performance of the solar cell. The TiO_2 films as prepared were annealed according to a programmed procedure: heating at 80 °C for 15 min; heating at 135 °C for 10 min; heating at 325 °C for 30 min; heating at 375 °C for 5 min; heating at 450 °C for 15 min; and heating at 500 °C for 15 min. The thickness of the transparent active layer was ~14 μm and that of the scattering layer ~5 μm. The TiO_2 films (active size 0.4 × 0.4 cm^2) as prepared were sensitized in a solution (N719 dye, Solaronix, 3 × 10^{-4} M) containing chenodeoxycholic acid (CDCA, 3 × 10^{-4} M) in acetonitrile/*tert*-butanol (v/v = 1 : 1) binary solvent for 8 h. After being washed with ethanol, the sensitized working electrode was assembled with a Pt counter electrode—CED-Pt or SD-Pt or TD-Pt—and sealed with a hot-melt film. An electrolyte solution (I_2 0.03 M; 4-*tert*-butylpyridine TBP, 0.5 M; 1,2-dimethyl-3-propylimidazolium iodide DMPII, 1.2 M; and guanidinium thiocyanate GuNCS, 0.1 M) in a mixture (v/v = 85/15) of acetonitrile (CH_3CN, 99.9%) and valeronitrile (n-C_4H_9CN, 99.9%) was used for all devices.

2.4 Device characterization

The current–voltage characteristics of the devices were measured with a digital source meter (Keithley 2400, computer-controlled) under one sun AM-1.5G irradiation from a solar simulator (SAN-EI, XES-502S) calibrated with a silicon-based reference cell (S1133, Hamamatsu). The spectra of the efficiency of

conversion of incident photons to current (IPCE) of the corresponding devices were recorded with a system comprising a Xe lamp (PTi A-1010, 150 W), a monochromator (PTi, 1200 g mm^{-1} blazed at 500 nm), and a source meter.

3. Results and discussion

3.1 Fabrications of Pt nanostructures

A CED technique is particularly useful to fabricate inorganic semiconductor nanostructures with crystalline and highly uniform size and shape.[40,41] According to a similar approach, the electro-deposition of Pt onto ITO glass *via* cyclic voltammetry (CV) scans was carried out on reducing H_2PtCl_6 in a solution containing $NaNO_3$, with the potential swept between −1.0 and 0.2 V (Fig. S2, ESI†). During the potential scan in the cathodic direction to −1.0 V, Pt(IV) ions from the precursor become reduced to Pt(II), followed by further reduction to form elemental Pt deposited on the ITO substrate with a cathodic maximum potential near −0.6 V. During the anodic scan in the other direction to +0.2 V, Pt becomes oxidized to Pt(II) with a small oxidation current to cause a slight dissolution of Pt that strips part of the Pt off the electrode. The CED process is highly irreversible because the rate of reduction is greater than the rate of oxidation through the CV scans. As a result, the formation of Pt nanostructures on the electrode becomes controlled through a subtle balance between deposition and dissolution.

Fig. 1 shows surface morphologies of the Pt nanostructures obtained with CED at $[H_2PtCl_6] = 5.0$ mM with varied deposition cycles: an apparent shape change is observed in these SEM images as the period of deposition gradually increases. At small periods of deposition (2 and 4 CV scans), the elemental Pt begins to form nanoclusters with irregular shape and a close-packed geometry (Fig. 1a and b). As the deposition periods increase (6 and 8 CV scans), the irregular nanoclusters aggregate to form a sheet-like nanostructure (Fig. 1c and d). A uniform morphology of the nanosheet structures—Pt-nanograss—standing vertically on the substrate was obtained at 10 CV scans (Fig. 1e). Afterwards, the uniform nanograsses begin to aggregate to form nanoflower-like structures when deposition cycles attain 15 scans. The inset of Fig. 1f displays a magnified image of a typical nanoflower fortuitously produced under these conditions with features mimicking a 'snow lotus flower'.

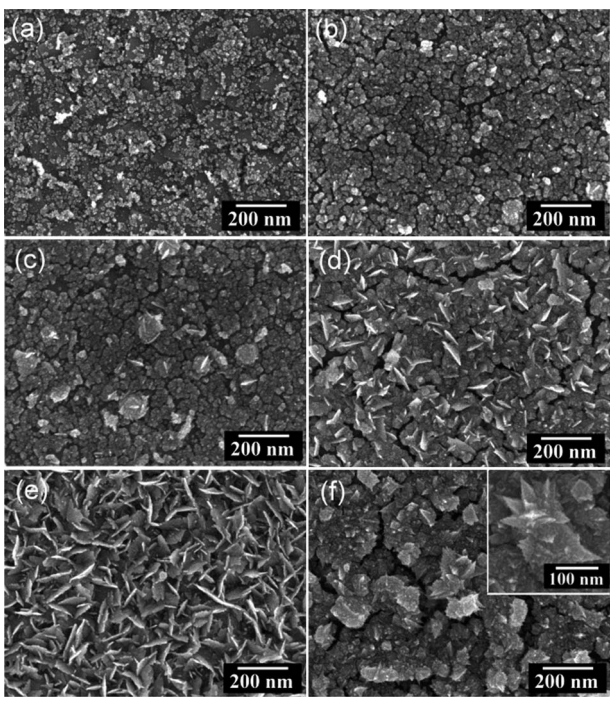

Fig. 1 FESEM top-view images of deposited Pt films obtained on cyclic electro-deposition (CED) with scan cycles (a) 2, (b) 4, (c) 6, (d) 8, (e) 10 and (f) 15. The inset in (f) shows a corresponding magnification of nanosheet aggregates with a nanoflower appearance.

Because a uniform Pt-nanograss structure was obtained at 10 CV scans, we performed further control experiments to examine the effect of the concentration of the Pt precursor (H_2PtCl_6) in synthetic solutions with deposition cycles fixed at 10 scans. Fig. 2 shows SEM images of Pt nanostructures with systematic morphological variation as the concentration of $[H_2PtCl_6]$ was varied in the range 1.0–12.5 mM. Similar to the variation of surface morphology shown in Fig. 1, Pt atoms aggregate to form nanoclusters (Fig. 2a and b) as the size of the nanoparticles increases with increasing concentration of the precursor in the range 1.0–1.5 mM. Nanosheet-like structures begin to appear at 2.5 mM (Fig. 2c); uniform nanograsses were obtained at 5 mM (Fig. 2d). Beautiful nanoflowers were produced at concentration 7.5 mM (Fig. 2e); they eventually formed a marvelous 'nanoflower sea' at concentration 12.5 mM (Fig. 2f). Fig. 2g–i show side views of the SEM images for a Pt layer produced at 1.0 (Fig. 2a), 5.0 (Fig. 2d) and 12.5 mM (Fig. 2f), respectively, for which the thickness of the Pt layer was systematically varied from 30 and 80 to 280 nm as the morphology of the nanostructures altered from nanocluster and nanograss to nanoflower. The side view of the nanoflower shown in Fig. 2i displays a morphology that mimics a real blooming rose.

We have demonstrated that a morphological control of the platinum nanostructure is achievable on varying either the period of electro-deposition or the concentrations of the precursor in the presence of $NaNO_3$. The role of the $NaNO_3$ salt in the shape control of Pt nanostructures must be justified. For this purpose, we performed a control experiment with an electrolyte solution containing H_2PtCl_6 (5 mM) and KCl (5 mM) in the absence of $NaNO_3$ at 10 CV scans. In the absence of $NaNO_3$, even though the same amount of the KCl salt was added, we observed no formation of Pt nanosheet/nanograss structures using the same CED procedure; only irregular Pt nanoparticles and nanoclusters were formed instead under these conditions (Fig. S3, ESI†), indicating that the $NaNO_3$ is involved in the construction of the sheet-like morphology and the formation of fascinating nanograss and nanoflower structures reported herein. The reasons for the observed $NaNO_3$ effect on the shape control of the Pt nanostructures are the following. Pileni pointed out that nanocrystal morphology is controllable in the presence of various anions selectively adsorbed on facets during crystal growth.[42] Xia and co-workers reported that the shape and size of Pt nanoparticles are controllable through the reduction kinetics with varied amounts of $NaNO_3$ in a polyol process;[43] they proposed that the formation of stable complexes between the Pt(II)/Pt(IV) species and nitrite anions in solution might cause a decreased rate of reduction of the Pt(IV) precursor for

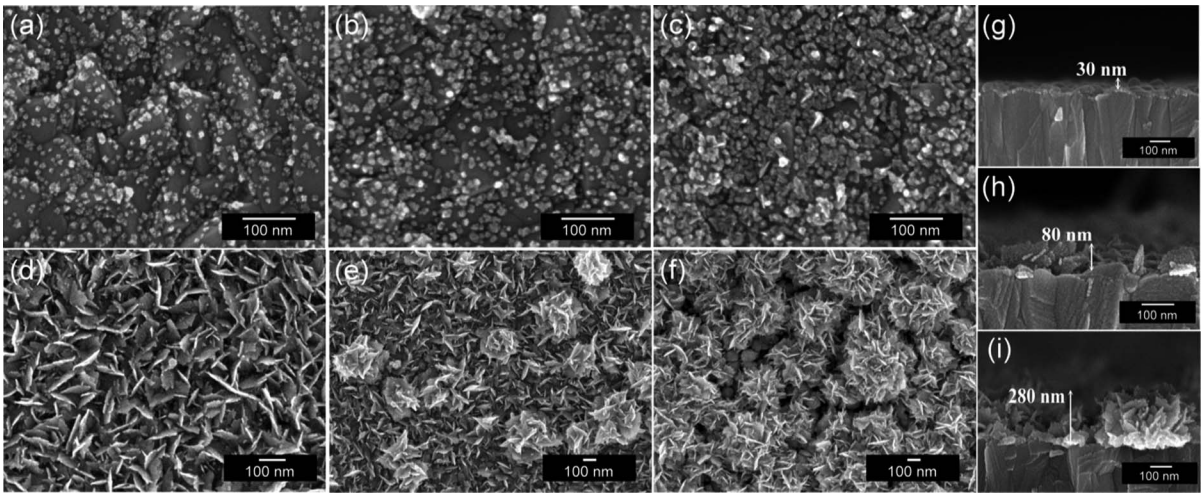

Fig. 2 FESEM top-view images of deposited Pt films obtained on cyclic electro-deposition (CED) with $[H_2PtCl_6]$ at concentrations per mM = (a) 1, (b) 1.5, (c) 2.5, (d) 5, (e) 7.5 and (f) 12.5; the cross-section images of Pt electrodes corresponding to the films (a), (d) and (f) show thickness L (nm) = (g) 30, (h) 80, and (i) 280, respectively, of the Pt layer.

anisotropic growth of the nanostructures to occur on certain facets. Lei and co-workers fabricated Pt-nanoflowers on a SWCNT membrane using CED in solution containing H_2PtCl_6 (1 mM) and H_2SO_4 (0.1 M);[44] they found that each Pt-nanoflower comprises many nanosheets growing anisotropically along the {111} direction. The suppression of the precursor reduction in a CED process is thus expected to be in the facet perpendicular to the {111} plane so that one observes the formation of two-dimensional nanosheet-like structures in the presence of $NaNO_3$.

3.2 Electro-catalytic activity of Pt electrodes

The catalytic function of Pt is strongly affected by the morphology of nanostructures; the Pt nanoparticles with 2D shapes gave the best catalytic performance.[45] Although beautiful Pt-nanoflowers were readily produced with the precursor at large concentrations, they were too fragile, and adhered poorly to the ITO substrate, for use as a high-performance CE for DSSC applications. Moreover, the Pt-nanoclusters prepared with small number of cycles show poorer catalytic activity and device performance than those obtained by thermal decomposition (Fig. S4, ESI†). For these reasons, we applied platinized electrodes with a uniform nanograss structure (CED-Pt) to examine the photovoltaic and electrochemical properties of the devices. For comparison with conventional platinized counter electrodes, we fabricated SD-Pt and TD-Pt electrodes by sputtering deposition and thermal decomposition, respectively, under corresponding optimized conditions described in the Experimental section and ESI†. The electro-catalytic activities of these Pt electrodes with respect to the tri-iodide reduction were investigated with CV and electrochemical impedance spectroscopy (EIS).[46] Fig. 3a shows cyclic voltammograms of various Pt films as working electrodes in acetonitrile solution. All cyclic voltammograms feature two anodic peak currents (I_{pa1} and I_{pa2}) and two cathodic peak currents (I_{pc1} and I_{pc2}). For the I_3^- reduction occurring on the CE surface, the larger cathodic peak current of CED-Pt (I_{pc2} = 1.43 mA cm^{-2}) reveals enhanced electro-catalytic activity of the electrode compared to SD-Pt, I_{pc2} = 1.14 mA cm^{-2}, and TD-Pt, I_{pc2} = 1.16 mA cm^{-2}. The small potential difference, $|\Delta E|$ = 0.31 V, between E_{pc2} and E_{pa1} of the CED-Pt electrode indicates a small polarization overpotential at the surface of the electrode, relative to the other two electrodes. The superior electro-catalytic performance of the CED-Pt electrode results from its small *charge-transfer overpotential*[11] reflecting the activation barrier of the interfacial charge transfer between the surface electrons in the electrode and I_3^- anions in the electrolyte, explained below.

The large electro-catalytic activity of the CED-Pt electrode was confirmed by the EIS[10,11,15] results shown in Fig. 3b. The impedance data were fitted according to an equivalent circuit shown in the inset of Fig. 3b with the key parameters summarized in Table 1. The first semicircle in the high-frequency domain represents the impedance of charge transfer at the electrode/electrolyte interface; the second semicircle in the low-frequency domain (not shown for SD-Pt and TD-Pt) reflects the

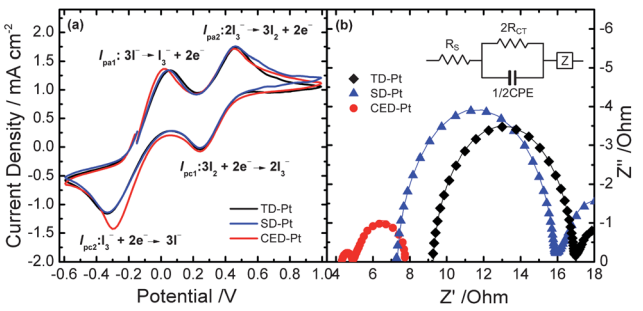

Fig. 3 (a) Cyclic voltammograms of platinized electrodes prepared with CED (red curves), SD (blue curves), and TD (black curves) in CH_3CN solution (LiI 0.01 M, I_2 0.001 M, and $LiClO_4$ 0.1 M) at scan rate 100 mV s^{-1}. (b) Nyquist plots obtained from electrochemical impedance spectroscopy (EIS) for symmetric cells composed of TD-TD (◆), SD-SD (▲) and CED-CED (●) Pt electrodes in the frequency range 10 mHz to 0.2 MHz. The inset shows the equivalent circuit scheme used in analysis of EIS results with impedance simulations at the electrode/electrolyte interface represented with series resistance R_S, charge-transfer resistance R_{CT} and chemical capacitance CPE.

Table 1 Photovoltaic parameters of DSSC devices under AM 1.5G one sun irradiation with active area 0.16 cm^2 and key EIS resistances of the corresponding platinized counter electrodes for devices constructed with a symmetric structure and active area 0.2 cm^2

Counter electrodes	J_{SC}/mA cm^{-2}	V_{OC}/V	FF	η (%)	R_S/Ω	R_{CT}/Ω
CED-Pt	15.10	0.818	0.778	9.61	4.3	0.3
SD-Pt	14.51	0.810	0.746	8.77	7.3	4.3
TD-Pt	13.71	0.822	0.759	8.55	9.3	3.8

contribution of Nernst diffusion in the solution. We focus on an analysis of the first semicircles of the EIS data, which show the charge-transfer resistances R_{CT} (Ω) = 0.3, 4.3 and 3.8 for symmetric cells based on CED-Pt, SD-Pt and TD-Pt, respectively. As expected, the R_{CT} of the TD-Pt film is slightly smaller than that of the SD-Pt film, but the CED-Pt electrode shows a much smaller R_{CT}, indicating that the electro-catalytic ability of CED-Pt is significantly greater than the others because of its greater intrinsic catalytic activity and the highly active surface area resulting from the unique platinum nanostructural morphology. The series resistances, R_S (Ω) = 4.3, 7.3 and 9.3 for CED-Pt, SD-Pt and TD-Pt, respectively, are related to the conductivity of the electrodes. The TD-Pt film shows the largest R_S because poor thermal stability of the ITO film causes increased resistance during reduction at 380 °C. The CED-Pt film reveals the smallest R_S because of the larger surface area and strong adhesion to the ITO substrate to improve the conductivity.[29] The observed small values of both R_{CT} and R_S for the CED-Pt electrode imply that the fill factor of the device is improved substantially when it is used as a CE for a DSSC.

3.3 Reflectivity of Pt electrodes

Upon photo-excitation, the dye molecules might not capture incident photons completely; the residual light reflected by the counter electrode might improve the efficiency of light harvesting. Nanograss structures, such as those shown in Fig. 1 and 2, have a sheet-like feature to scatter residual light effectively for enhanced light harvesting. The light-reflecting properties of the CE made of CED-Pt, SD-Pt and TD-Pt were evaluated from reflection spectra. As shown in Fig. 4, the TD-Pt film without a mirror-like surface has a reflectivity <20% because the particles are small and the packing is sparse as indicated in the SEM images (Fig. S5, ESI†). The CED-Pt film shows reflectivity of 40–50% in the spectral range 400–800 nm that includes the absorption by most organic dyes. The inset of Fig. 4 shows a clear mirror image reflected by the CED-Pt substrate, visualizing the great reflectivity of the film. To prepare a SD-Pt film with a reflectivity comparable to that of the CED-Pt film, we employed a sputtering period of 5.5 min (Fig. S6, ESI†) to produce a continuous and densely packed Pt film, but a sputtering duration of only 15 s sufficed to produce a SD-Pt CE with effective electro-catalytic activity, indicating that only platinum deposited near the surface contributes effectively to the electro-catalytic function. A mirror-like SD-Pt film with reflectivity similar to that of the CED-Pt film is hence not beneficial to improve the electro-catalytic performance; to the contrary, it suffers from extra and expensive platinum sputtered to deposit

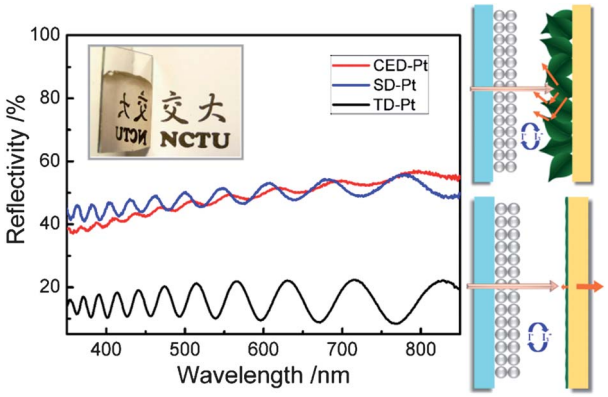

Fig. 4 Left panel: reflection spectra of Pt films fabricated with CED (red curve), SD (blue curve), and TD (black curve); the inset shows a mirror-image photograph of the CED-Pt electrode with nanograss structure. Right panel: schematic representation of DSSC structures showing the scattering of incident light with reflective (top) and transparent (bottom) counter electrodes.

the film. Instead of a densely packed structure of the SD-Pt film, the CED-Pt film features sheet-like nanostructures that provide a large surface area to scatter effectively the incident light. The right part of Fig. 4 shows schematically the scattering function of a sheet-like nanograss film. The highly reflective CED-Pt film is expected to enhance the light-harvesting efficiency of the device to increase the photocurrent.

3.4 Photovoltaic performance of DSSC devices

The same platinum counter electrodes were integrated into DSSC devices under the same experimental conditions. The current–voltage characteristics and the corresponding IPCE action spectra of these devices are shown in Fig. 5; the corresponding photovoltaic parameters are summarized in Table 1. V_{OC} values of the three devices are similar, but J_{SC} (CED-Pt > SD-Pt > TD-Pt) and FF (CED-Pt > TD-Pt > SD-Pt) exhibit

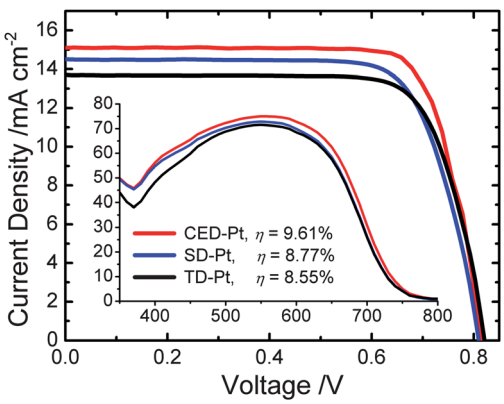

Fig. 5 Current–voltage characteristics and the corresponding IPCE action spectra (external quantum efficiencies in percentage *vs.* wavelength in nm) of N719-based DSSC devices under simulated AM 1.5G solar illumination at 100 mW cm^{-2} with active area 0.16 cm^2. The devices were fabricated according to the same materials and experimental procedures except with Pt counter electrodes constructed with CED (red), SD (blue) and TD (black).

systematic trends. Because the magnitude of the FF depends strongly on the electro-catalytic activity reflected by the value of R_{CT}, the order of the FF is consistent with the variation of R_{CT} showing the opposite trend. The FF, 0.746, of the SD-Pt device is smaller than that, 0.759, of the TD-Pt device because the former exhibits a poorer electro-catalytic activity than the latter due to the densely packed structure of the former, but the excellent scattering effect of the SD-Pt device of which the greater reflectivity enhances its light-harvesting efficiency yields J_{SC} = 14.51 mA cm^{-2} whereas for the TD-Pt device, it is 13.71 mA cm^{-2}. With balanced performances of FF and J_{SC} for both SD-Pt and TD-Pt devices, similar efficiencies, 8.77 and 8.55%, of power conversion were attained. For the CED-Pt device with a nanograss structure, the excellent electro-catalytic activity reflects its charge-transfer resistance R_{CT} = 0.3 Ω, increasing its FF value to 0.778. Such an excellent electro-catalytic effect is considered to release I^- species rapidly from the electrolytic reduction at the electrode/electrolyte interface, so as to enhance the dye regeneration and to improve the efficiency of charge collection to increase its J_{SC}. With consideration of the excellent light-scattering effect to improve the light-harvesting efficiency, the DSSC device made of CED-Pt CE exhibits J_{SC} = 15.10 mA cm^{-2}, superior to other devices. The overall power conversion efficiency of the CED-Pt device attains 9.61%, a performance enhanced 12% relative to that of a conventional TD-Pt device under the same fabrication conditions.

Although impressive photovoltaic performance has been reported with novel sensitizers and electrode materials, it is essential to develop devices with superior long-term stability and outstanding performance. We therefore made an attempt to optimize the cell performance for the DSSC devices with thicker nanocrystalline TiO_2 films (17 + 5 μm) sensitized with thermally stable amphiphilic ruthenium dye [RuLL'(NCS)$_2$] (L = H_2dcbpy = 2,2′-bipyridine-4,4′-dicarboxylic acid, L′ = dnbpy = 4,4′-dinoyl-2,2′-bipyridine) known as Z907.[47] Fig. 6 shows the optimized current–voltage characteristics of the DSSC devices fabricated using the CED-Pt and TD-Pt films as counter electrodes. The results display a consistent trend for both J_{SC} and FF, in which the current densities and the fill factors significantly increase from J_{SC} = 18.51 mA cm^{-2} and FF = 0.719 (the TD-Pt device) to J_{SC} = 19.44 mA cm^{-2} and FF = 0.736 (the CED-Pt device); the corresponding power conversion efficiencies increase from 9.77% to 10.62%, which is unprecedented for the Z907-sensitized solar cell with great long-term stability.[47,48]

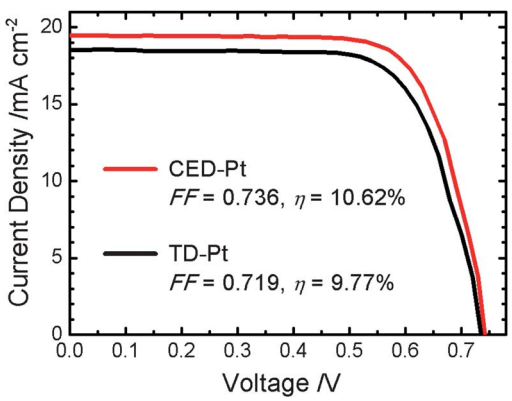

Fig. 6 The current–voltage characteristics of the DSSC devices fabricated with CED-Pt (red) and TD-Pt (black) counter electrodes. The device performances were optimized with thicker TiO_2 films (17 + 5 μm) sensitized with dye Z907.

4. Conclusions

In conclusion, we report a novel solution-phase technique to fabricate nanostructured Pt electrodes according to a cyclic electro-deposition approach in the presence of $NaNO_3$. The platinum layer on the ITO surface is controllable to show varied nanocluster, nanosheet, nanograss, and nanoflower morphologies on adjusting the cycles of CED scans or the initial concentration of the H_2PtCl_6 precursor. We applied CV and EIS techniques to study the electro-catalytic activity of the electrodes; the electro-catalytic performance of the Pt electrode with nanograss feature is superior to those made of sputtering deposition and conventional thermal decomposition. When these Pt electrodes were fabricated into DSSC devices under the same experimental conditions, the CED-Pt device exhibited the best cell performance. The excellent performance—FF = 0.778 and J_{SC} = 15.10 mA cm^{-2}—of the CED-Pt device is due to the improved electro-catalytic activity with charge-transfer resistance of only 0.3 Ω and the intrinsic light-scattering effect with a large surface area for reflectivity of ~50%. The CED technique thus provides a promising approach to fabricate a cost-effective counter electrode with brief deposition for highly efficient applications in solar cells. The presented CED-Pt electrode has the advantages of processing at low temperature with a small Pt-loading and an effective catalytic performance, giving it the potential for application in plastic electrodes for flexible photovoltaic applications. Other potential applications of these Pt-nanomaterials include heterogeneous catalysis, control of vehicle emission, production of hydrogen, sensors and fuel cells.

Acknowledgements

National Science Council of Taiwan and Ministry of Education of Taiwan, under the ATU program, provided support for this project.

Notes and references

1 M. Grätzel, *Acc. Chem. Res.*, 2009, **42**, 1788.
2 H. J. Snaith, *Adv. Funct. Mater.*, 2010, **20**, 13.
3 A. Hagfeldt, G. Boschloo, L. Sun, L. Kloo and H. Pettersson, *Chem. Rev.*, 2010, **110**, 6595.
4 Z. Ning, Y. Fu and H. Tian, *Energy Environ. Sci.*, 2010, **3**, 1170.
5 A. Mishra, M. K. R. Fischer and P. Bäuerle, *Angew. Chem., Int. Ed.*, 2009, **48**, 2474.
6 M. V. Martínez-Díaz, G. Torre and T. Torres, *Chem. Commun.*, 2010, **46**, 7090.
7 A. Yella, H.-W. Lee, H. N. Tsao, C. Yi, A. K. Chandiran, M. K. Nazeeruddin, E. W.-G. Diau, C.-Y. Yeh, S. M. Zakeeruddin and M. Grätzel, *Science*, 2011, **334**, 629.
8 L.-L. Li, C.-Y. Tsai, H.-P. Wu, C.-C. Chen and E. W.-G. Diau, *J. Mater. Chem.*, 2010, **20**, 2753.
9 O. K. Varghese, M. Paulose and C. A. Grimes, *Nat. Nanotechnol.*, 2009, **4**, 592.
10 N. Papageorgiou, W. F. Maier and M. Grätzel, *J. Electrochem. Soc.*, 1997, **144**, 876.
11 N. Papageorgiou, *Coord. Chem. Rev.*, 2004, **248**, 1421.
12 T. N. Murakami and M. Grätzel, *Inorg. Chim. Acta*, 2008, **361**, 572.
13 A. Hauch and A. Georg, *Electrochim. Acta*, 2001, **46**, 3457.

14 C. M. Chen, C. H. Chen and T. C. Wei, *Electrochim. Acta*, 2010, **55**, 1687.
15 L. Kavan, J. H. Yum and M. Grätzel, *ACS Nano*, 2011, **5**, 165.
16 P. Joshi, L. Zhang, Q. Chen, D. Galipeau, H. Fong and Q. Qiao, *ACS Appl. Mater. Interfaces*, 2010, **2**, 3572.
17 W. J. Lee, E. Ramasamy, D. Y. Lee and J. S. Song, *ACS Appl. Mater. Interfaces*, 2009, **1**, 1145.
18 M. Wu, X. Lin, T. Wang, J. Qiub and T. Ma, *Energy Environ. Sci.*, 2011, **4**, 2308.
19 J. Wu, Q. Li, L. Fan, Z. Lan, P. Li, J. Lin and S. Hao, *J. Power Sources*, 2008, **181**, 172.
20 Q. W. Jiang, G. R. Li and X. P. Gao, *Chem. Commun.*, 2009, 6720.
21 M. Wang, A. M. Anghel, B. Marsan, N.-L. Cevey Ha, N. Pootrakulchote, S. M. Zakeeruddin and M. Grätzel, *J. Am. Chem. Soc.*, 2009, **131**, 15976.
22 G. R. Li, F. Wang, Q. W. Jiang, X. P. Gao and P. W. Shen, *Angew. Chem., Int. Ed.*, 2010, **49**, 3653.
23 H. Sun, D. Qin, S. Huang, X. Guo, D. Li, Y. Luo and Q. Meng, *Energy Environ. Sci.*, 2011, **4**, 2630.
24 M. Wu, X. Lin, A. Hagfeldt and T. Ma, *Angew. Chem., Int. Ed.*, 2011, **50**, 3520.
25 X. Fang, T. Ma, G. Guan, M. Akiyama, T. Kida and W. Abe, *J. Electroanal. Chem.*, 2004, **570**, 257.
26 Y.-L. Lee, C.-L. Chen, L.-W. Chong, C.-H. Chen, Y.-F. Liu and C.-F. Chi, *Electrochem. Commun.*, 2010, **12**, 1662.
27 L.-Y. Lin, P.-C. Nien, C.-P. Lee, K.-W. Tsai, M.-H. Yeh, R. Vittal and K.-C. Ho, *J. Phys. Chem. C*, 2010, **114**, 21808.
28 S.-S. Kim, Y.-C. Nah, Y.-Y. Noh, J. Jo and D.-Y. Kim, *Electrochim. Acta*, 2006, **51**, 3814.
29 C. H. Yoon, R. Vittal, J. Lee, W.-S. Chae and K.-J. Kim, *Electrochim. Acta*, 2008, **53**, 2890.
30 Y.-J. Song, J.-K. Oh and K.-W. Park, *Nanotechnology*, 2008, **19**, 355602.
31 C.-M. Chena, C.-H. Chena, S.-J. Chernga and T.-C. Wei, *Mater. Chem. Phys.*, 2010, **124**, 173.
32 K. Sun, B. Fan and J. Ouyang, *J. Phys. Chem. C*, 2010, **114**, 4237.
33 L. Chen, W. Tan, J. Zhang, X. Zhou, X. Zhang and Y. Lin, *Electrochim. Acta*, 2010, **55**, 3721.
34 G. Calogero, P. Calandra, A. Irrera, A. Sinopoli, I. Citro and G. D. Marco, *Energy Environ. Sci.*, 2011, **4**, 1838.
35 B. Lee, D.-K. Hwang, P. Guo, S.-T. Ho, D. B. Buchholtz, C.-Y. Wang and R. P. H. Chang, *J. Phys. Chem. B*, 2010, **114**, 1458.
36 M. K. Nazeeruddin, A. Kay, I. Rodicio, R. Humphry-Baker, E. Müller, P. Liska, N. Vlachopoulos and M. Grätzel, *J. Am. Chem. Soc.*, 1993, **115**, 6382.
37 H. J. Snaith, A. J. Moule, C. Klein, K. Meerholz, R. H. Friend and M. Grätzel, *Nano Lett.*, 2007, **7**, 3372.
38 L.-Y. Lin, C.-P. Lee, R. Vittal and K.-C. Ho, *J. Power Sources*, 2010, **195**, 4344; L.-Y. Lin, C.-P. Lee, R. Vittal and K.-C. Ho, *J. Power Sources*, 2011, **196**, 1671.
39 S. Ito, P. Chen, P. Comte, M. K. Nazeeruddin, P. Liska, P. Péchy and M. Grätzel, *Progr. Photovolt.: Res. Appl.*, 2007, **15**, 603; S. Ito, T. N. Murakami, P. Comte, P. Liska, C. Grätzel, M. K. Nazeeruddin and M. Grätzel, *Thin Solid Films*, 2008, **516**, 4613.
40 A. M. Kressin, V. V. Doan, J. D. Klein and M. J. Sailor, *Chem. Mater.*, 1991, **3**, 1015.
41 Y. Yang, S. C. Kung, D. K. Taggart, C. Xiang, F. Yang, M. A. Brown, A. G. Güell, T. J. Kruse, J. C. Hemminger and R. M. Penner, *Nano Lett.*, 2008, **8**, 2447.
42 M.-P. Pileni, *Nat. Mater.*, 2003, **2**, 145.
43 T. Herricks, J. Chen and Y. Xia, *Nano Lett.*, 2004, **4**, 2367.
44 L. Su, W. Jia, L. Zhang, C. Beacham, H. Zhang and Y. Lei, *J. Phys. Chem. C*, 2010, **114**, 18121.
45 S. Mostafa, F. Behafarid, J. R. Croy, L. K. Ono, L. Li, J. C. Yang, A. I. Frenkel and B. R. Cuenya, *J. Am. Chem. Soc.*, 2010, **132**, 15714.
46 F. Fabregat-Santiago, G. Garcia-Belmonte, I. Mora-Seró and J. Bisquert, *Phys. Chem. Chem. Phys.*, 2011, **13**, 9083.
47 P. Wang, S. M. Zakeeruddin, P. Comte, R. Charvet, R. Humphry-Baker and M. Grätzel, *J. Phys. Chem. B*, 2003, **107**, 14336.
48 Q. Yu, S. Liu, M. Zhang, N. Cai, Y. Wang, P. Wang, S. M. Zakeeruddin, P. Comte, R. Charvet, R. Humphry-Baker and M. Grätzel, *J. Phys. Chem. C*, 2009, **113**, 14559.